Engineered Science

RESEARCH PAPER

View Article Online

Biomass-derived nitrogen-doped porous carbons (NPC) and NPC/polyaniline composites as high performance supercapacitor materials

Xizhi Wang,† Xiaofei Zeng† and Dapeng Cao*

Currently, developing high performance supercapacitor material suitable for application in the areas which require high energy density battery, is still a great challenge. Here we use biomass poplar sawdust as precursors to prepare nitrogen-doped porous carbons (NPC) and the NPC/polyaniline (PANI) composites, and further explore its application in supercapacitor electrodes. By optimizing the carbonization temperature, we find the NPC-750 sample shows a highest specific capacitance of 362 $F{\cdot}g^{-1}$ in 6 M KOH at 0.5 $A{\cdot}g^{-1}$ among the four samples, due to its large specific surface area of 2149 $m^2{\cdot}g^{-1,}$ and suitable pore size distribution and high graphitization degree. Further investigations indicate that NPC/PANI composite exhibits a much higher specific capacitance of 312 $F{\cdot}g^{-1}$ than 252 $F{\cdot}g^{-1}$ of NPC at 5 $A{\cdot}g^{-1}$, and a wider voltage range of 0-1.4 V than the one of 0-1V of NPC, as well as a much higher energy density of 15.45 $Wh{\cdot}kg^{-1}$, which is 2.73 times of 5.66 $Wh{\cdot}kg^{-1}$ of NPC. This work indicates that integrating porous carbon and PANI into a composite is a promising strategy for developing high performance supercapacitor electrode materials.

Keywords: Nitrogen-doped porous carbons; Energy storage and conversion; Biomass waste reutilization; Polymer composites

Received 15th March 2018, Accepted 25th March 2018

DOI: 10.30919/es.180325

1. Introduction

With the fast consumption of traditional fossil fuels (e.g. coal and oil and nature gas) and the growing energy requirement of the current society, it is an urgent task to develop high efficient, inexpensive and environmentally friendly conversion technologies and energy storage systems.[1,2] Recently, development of energy storage devices such as batteries and supercapacitors has received more and more attention. Compared with traditional batteries, supercapacitor is a new type of electrochemical energy storage cell with high power density and excellent cycling stability. It can be charged–discharged in a matter of seconds and almost no pollution to the environment, and is very suitable for applying in the areas which require high power density batteries.[3–8] Therefore, developing high performance supercapacitor materials is a current hot topic.

According to the different charge-storage mechanism, supercapacitors can be categorized into two categories: electrical double-layer capacitors (EDLCs) and Faradaic capacitors.[9] Faradaic capacitors are primarily dominated by reversible redox reactions at the surface of the electrode materials,[10] and the frequently used electrode materials contain metal oxides,[11] functionalized carbon powders[12] and conducting polymers,[13] while EDLCs store energy by accumulating electrostatic charge in the electric double layers at the electrode/electrolyte interface, and no electrochemical reaction occurs in the process.[14] Activated carbon,[15] carbon nanotube,[16] carbon aerogels,[17] graphene[18,19] and carbide-derived carbons,[20] have been widely considered as EDLCs electrode materials, owing to their chemical and thermal stability, high specific surface area, desirable electric conductivity and relatively low cost.[5,18,21] Recently, the composite materials combining the EDLCs and Faradaic capacitance have been proposed to accomplish the performance beyond the limitations of each material,[22] such as carbon/conducting polymer composites[23,24] and carbon/metal oxide composites.[25,26]

Currently, using metal-organic framework (MOF),[18,21] biomass[27–29] and other hard template[30] as precursors to obtain porous carbons has been reported extensively.[31,32] Compared to MOF and hard templates, biomass precursors show a lot of advantages, such as low cost, specific texture structure by natural selection and easy accessibility.[29] Moreover, using biomass as precursors to obtain porous carbon can achieve reutilization of waste biomass and avoid traditional plant waste burning which often causes severe environmental pollutions and even leads to the fog and haze weather. Therefore, it is significantly important to use waste biomass as precursors to synthesize the porous carbons for supercapacitor application.

Previous investigations have reported a series of biomass-derived porous carbons and their applications in supercapacitors. Willow catkins,[29] waste celtuce leaves,[33] chicken eggshell membranes,[34] eggplants[35] and natural crab shell[36] as highly accessible waste biomass sources, have been used to prepare the corresponding activated carbons by KOH activation process, and these as-

State Key Laboratory of Organic-Inorganic Composites, and Beijing Advanced Innovation Center for Soft Matter Science and Engineering, Beijing University of Chemical Technology, Beijing 100029, People's Republic of China. E-mail: caodp@mail.buct.edu.cn
† Equally contributed to this work

synthesized samples show the capacitance of about 300 F/g in alkaline electrolytes.[37] These investigations indicate that KOH is a good activating reagent,[38–40] and the proper precursor, activation agent and preparation method would synergistically affect the electrochemical properties of the synthesized porous carbons.[9] Although activated carbon is the most widely used materials for supercapacitor due to its high specific surface area, excellent chemical stability and high conductivity,[41] most activated carbon suffers from poor rate performance because of the insufficient ion diffusion within the micropores, which limits their energy density (5–8 $Wh{\cdot}kg^{-1}$) and power density.[42]

Polyaniline (PANI) was considered as one of the most attractive materials due to its easy synthesis, low cost and high electrical conductivity.[43,44] Recently, PANI has been widely used to prepare carbon/PANI composites for improving supercapacitor performance, especially the power and energy densities.[35,45,46] Gupta et al. prepared a PANI/SWCNT composite with a specific capacitance of 463 $F{\cdot}g^{-1}$.[47] Li et al. reported a carbon/PANI composite with specific capacitance of 747 $F{\cdot}g^{-1}$ at a current density of 0.1 $A{\cdot}g^{-1}$.[48] Uppugalla et al. also found that heteroatom-doped carbon (CNSO)/PANI composite yielded a higher capacitance of 372 $F{\cdot}g^{-1}$ than CNSO.[49] Moreover, Yu et al reported that HPC/PANI nanowire composite exhibits a voltage window of 0–1.8 V, a high energy density of 60.3 $Wh{\cdot}kg^{-1}$ and power density of 18 $kW{\cdot}kg^{-1}$ in 1 M Na_2SO_4.[41] All above these studies indicate that the synergistic effects between carbon materials and PANI could enhance the specific capacitance of carbon materials significantly.

In this work, we first synthesize nitrogen-doped porous carbons (NPC) by using biomass poplar sawdust as precursors. By exploring the effects of temperature on the as-synthesized samples, we screen an optimal carbon sample NPC-750 to further prepare the NPC/PANI composites by *in situ* polymerization of aniline on it. Then, the voltage range and energy density of the NPC/PANI composites were studied. Finally, conclusions were drawn and the discussion was addressed.

2. Results and Discussion

Scheme 1 shows the illustration of preparation of NPC and NPC/PANI composites. First, the raw sawdust was washed by 1 M HCl and water and then dried in an oven. The dried sample was grinded into powder and mixed with KOH powder in solid phase for further carbonization at different temperatures (T=650, 700, 750, 800°C) for 3 h in argon atmosphere. The obtained carbon materials were marked as NPC-X, where X indicates the activation temperature. Subsequently, the prepared carbons were washed by 1 M HCl and water and dried in an oven. The selected NPC was further used to prepare the NPC/PANI composites by *in situ* polymerization of aniline monomer on NPC material. The detailed synthesis and characterization were presented in Supporting Information.

Figure 1 shows the SEM and TEM images of four poplar sawdust-derived N-doped porous carbon samples. Apparently, the SEM and TEM images of all the four samples exhibit a sheet-like structure, and there is no obvious difference, which may be attributed to the fact that the organics in biomass was decomposed almost completely.[33] The SEM elemental mapping of a randomly selected sample is shown in Figure S1, which reveals the C, O and N elements distribute uniformly over the entire material.

To further explore the structure of as-synthesized samples, Raman spectra were carried out and shown in Figure 2a. Two characteristic Raman bands at 1592 cm^{-1} (G band) and 1355 cm^{-1} (D band) can be clearly observed. The former is related to the graphitic order, while the latter is connected with amorphous structure.[50] The graphitization degree of porous carbons is widely evaluated by the ratio of relative intensity between G and D bands (IG/ID).[51] The I_G/I_D ratios of NPC-650, -700, -750 and -800 samples are about 1.14, 1.15, 1.39 and 1.06 (also see Table S1), respectively. Obviously, the IG/ID value of NPC-750 is the highest, indicating that 750°C is a best temperature for yielding high graphitization sample. To reveal the possible reasons, we also performed the thermogravimetric analysis (TGA) of precursor (i.e. the mixture of poplar sawdust and KOH in 1: 2 weight ratio) in flowing N_2. Figure 2b shows a significant weight loss

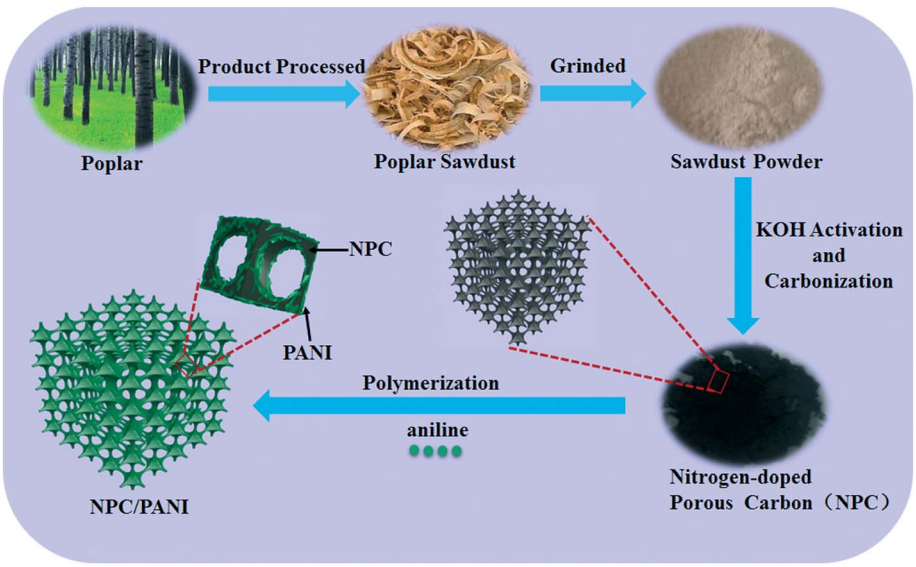

Scheme 1 Schematic illustration of the preparation of poplar sawdust-derived nitrogen-doped porous carbons (NPC) and NPC/PANI Composites.

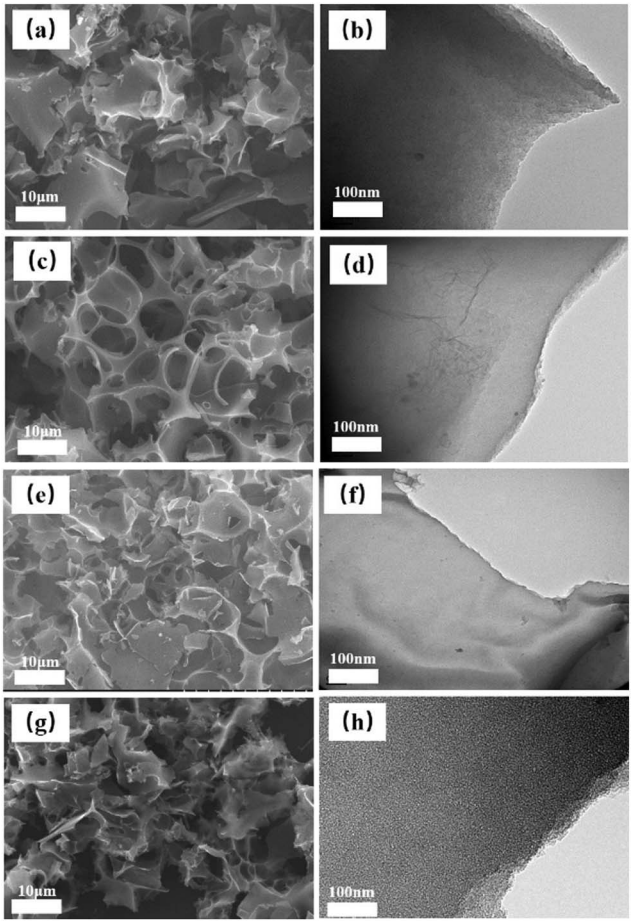

Fig. 1 Morphologies of four poplar sawdust-derived nitrogen-doped porous carbons. Left panel: SEM images, Right panel: TEM images. (a, b) NPC-650, (c, d) NPC-700, (e, f) NPC-750, (g, h) NPC-800.

in T<200 °C, which may be mainly related to the elimination of various volatiles (e.g. water). However, when T> 750 °C, the weight loss is obvious, which may be mainly related to partial decomposition of samples at the high temperature,[52] suggesting that 750 °C is a suitable temperature for graphitization of samples, which is consistent with the result of Raman spectra.

Figure 2c and 2d show adsorption isotherms of N_2 at 77 K and pore size distribution (PSD) of four samples, where all four isotherms exhibit a typical type-I curve mainly containing micropores.[53] The BET specific surface areas of NPC-650, -700, -750 and -800 are 1005, 1245, 2149 and 1855 $m^2 \cdot g^{-1}$, and their pore volumes are about 0.44, 0.64, 0.97 and 0.95 $cm^3 \cdot g^{-1}$, respectively. Definitely, NPC-750 sample shows not only the highest adsorption amount, specific surface area and pore volume, but also a wide PSD (Figure 2d) containing micropore (<2 nm) and mesopore (2-3 nm). All these observations indicate that NPC-750 is a promising candidate for supercapacitor electrodes among the four samples.

XPS analysis in Figure 3a shows the existence of oxygen and nitrogen atoms in the as-synthesized samples. The partial magnification of the XPS spectra and the SEM elemental mapping further confirm the existence of nitrogen. The nitrogen sources in samples are from the accumulation in the natural growth of the poplar. As well known, the existence of nitrogen can significantly improve the electrochemical performance of the porous carbons[54–56] because the introduction of nitrogen would induce the surface charge redistribution of carbon materials.[8,57,58] The nitrogen contents of the four samples obtained from XPS were listed in Table 1. The content of the nitrogen mainly keeps in the range of 1.1~1.5 wt% for the three samples of NPC-650, -700, -750, while it is 0.79 wt% for NPC-800, possibly owing to the fact that high temperature leads to more nitrogen loss.[59]

The complex N1s spectra were also further resolved into three different peaks at 398.5, 400.1, and 401.5 eV, referring to pyridinic-N (N-6), pyrrolic-N (N-5) and quaternary-N (N-Q) in Figure 3b-3e and Table S2.[60,61] It is reported that N-6 and N-5 are beneficial for Faradaic pseudocapacitance, while N-Q is helpful for improving the conductivity of porous carbons.[18,62] As shown in the Figure 3f and Table S2, the contents of N-Q of NPC-650, -700, -750 and -800 are about 0.32%, 0.41%, 0.65% and 0, respectively, in which that the NPC-750 is also slightly higher than the other three samples.

The electrochemical properties of all the four carbon samples in 6 M KOH electrolyte in three-electrode system were measured. Figure 4a and 4b show the cyclic voltammograms (CV) at a scan rate of 25 $mV \cdot s^{-1}$ and galvanostatic charge (GC)–discharge curves at a current density of 0.5 $A \cdot g^{-1}$ of four samples, respectively. The CV curves show a similar quasi-rectangular shape, suggesting that the energy storage process is the typical electrical double-layer capacitors by accumulating electrostatic charge, and the GC curves show asymmetric process related to the pseudocapacitance. Obviously, NPC-750 exhibits a largest CV area and a highest specific capacitance among the four samples. The specific capacitances of four nitrogen-doped porous carbons at different current densities are presented in Figure 4c, and the detailed data are listed in Table S3, which is calculated by using the equation (S1) in Supporting Information. Actually, the high capacitance (362 $F \cdot g^{-1}$ at 0.5 $A \cdot g^{-1}$) of NPC-750 is not only larger than other there samples NPC-650 (272.9$F \cdot g^{-1}$), NPC-700 (301.5 $F \cdot g^{-1}$) and NPC-800 (231 $F \cdot g^{-1}$), but also higher than other porous carbons in literature, like ZIF-derived porous carbon (223 $F \cdot g^{-1}$ at 0.5 $A \cdot g^{-1}$),[18] carbonized eggshell membrane(261 $F \cdot g^{-1}$ at 0.5$A \cdot g^{-1}$),[34] hierarchical porous carbon microtubes (292 $F \cdot g^{-1}$ at 1 $A \cdot g^{-1}$)[29] and nitrogen-doped porous graphitic carbon (293 $F \cdot g^{-1}$ at 1 $A \cdot g^{-1}$).[60] Moreover, at 2$A \cdot g^{-1}$, the specific capacitance of NPC-750 still remains to be 275.6 $F \cdot g^{-1}$, indicating that NPC-750 holds a good rate capability.

Figure 4d shows the electrochemical impedance and equivalent circuit model of the four samples. In the high frequencies, all the carbons display a well-defined semicircle (see the inset in Figure 4d), while in the low frequencies, a nearly vertical curve appears. NPC-750 shows a smallest value crossing with the Z' axis, suggesting that it has lowest interface contact resistance among four samples, because its PSD is more suitable for fast diffusion of electrolyte ions. In the low frequency region, the vertical curve implies an ideal capacitive behavior.[63] The larger the curve slope, the better is the capacitive behavior. Obviously, NPC-750 exhibits the largest slope, meaning that it has the largest capacitance among four samples.

To quantitatively analyze the electrochemical properties, the equivalent circuit model of the four porous carbons was proposed

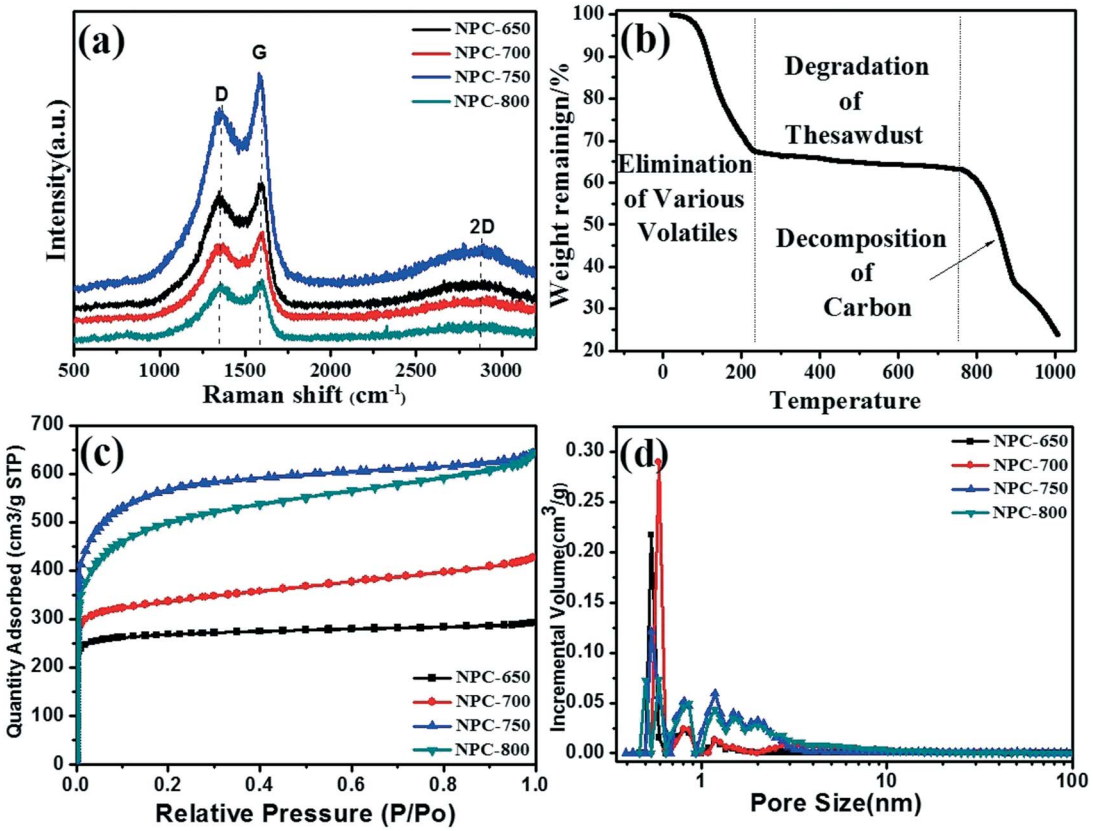

Fig. 2 (a) Raman spectra of four poplar sawdust-derived nitrogen-doped porous carbons, (b) TGA analysis of the precursor (poplar sawdust and KOH in the weight ratio of 1:2 10°C·min^{-1} in flowing N2), (c) Adsorption–desorption isotherms of N_2 of four samples at T=77 K, (d) Pore size distribution of four samples.

based on the literature from Wang et al.,[7] and shown in the inset of Figure 4d. The system is divided into three parts, including the bulk solution, the diffusion layer and the double layer.[64] In the equivalent circuit, it contains the bulk solution resistance (Rs), the contact interface resistance (Rc) and contact interface capacitance(Cc), ion diffusion Warburg resistance (Zw) and the double-layer capacitance (Cd) inside pores. Table S4 shows the results obtained by the analysis of the Nyquist plots, in which Rc of NPC-750 is smallest and Zw of NPC-750 is the lowest among four samples. As a result, the Cc and Cd of NPC-750 are the largest among the four samples. These results excellently agree with the quantitative analysis mentioned above.

To further explore the practical application of NPCs, the electrochemical properties of materials were also measured in a two-electrode system using 6 M KOH as the electrolyte. Figure 5a and 5b show the cyclic voltammograms at a scan rate of 25 mV·s^{-1} and galvanostatic charge–discharge curves at a current density of 0.5 A·g^{-1}, respectively. Obviously, NPC-750 still exhibits a largest CV area and specific capacitance among the four samples, which is consistent with the results in the three-electrode system. Figure 5c shows the specific capacitance of four nitrogen-doped porous carbons at different current densities, and the calculated capacitances of NPC-750 is 40.8 F·g^{-1} at a current density of 0.5 A·g^{-1}, which is higher than other three samples, and the capacitance of NPC-750 at different current densities is also higher than that of others, which is consistent with the three-electrode system. Figure 5d shows the Ragone plot (energy density 8 power density) of four nitrogen-doped porous carbons based on the active material weight. The maximum energy density of the carbon material is 5.66 Wh·kg^{-1} at 125 W·kg^{-1} and maintains 3.75 Wh·kg^{-1} at 2500 W·kg^{-1}, which is far from practical application requirements.

To improve the energy density of NPCs, the NPC/PANI composite were further synthesized via *in situ* polymerization on the NPC-750, because NPC-750 possesses the best electrochemical performance among four samples, and therefore was used as a scaffold for coating of PANI. The SEM image (Figure S2) shows that the PANI nanowire is evenly grown on the surface of NPC. Figure S3 shows the adsorption–desorption isotherms and PSDs of NPC and NPC/PANI samples. It can be observed that the surface area decreased remarkably owing to the filling effect of PANI to pore, and the NPC/PANI mainly contains mesoopore of 2.5-10 nm. The cyclic voltammograms of NPC/PANI composites at different scan rates were presented in Figure S4, where there is a reduction peak at -0.55 V and an oxidation peak at 0 V that are associated with the redox transition of PANI between the semiconducting state and conducting state.[44] This observation also indicates the existence of PANI in the composite. Other detailed characterizations including XPS, Raman and Nyquist impedance, were presented in Supporting Information.

The electrochemical properties of the composites in 6 M KOH electrolyte in three-electrode and two-electrode systems were measured. Figure 6a shows the galvanostatic charge–discharge of NPC/PANI at different current densities in three-electrode. It can

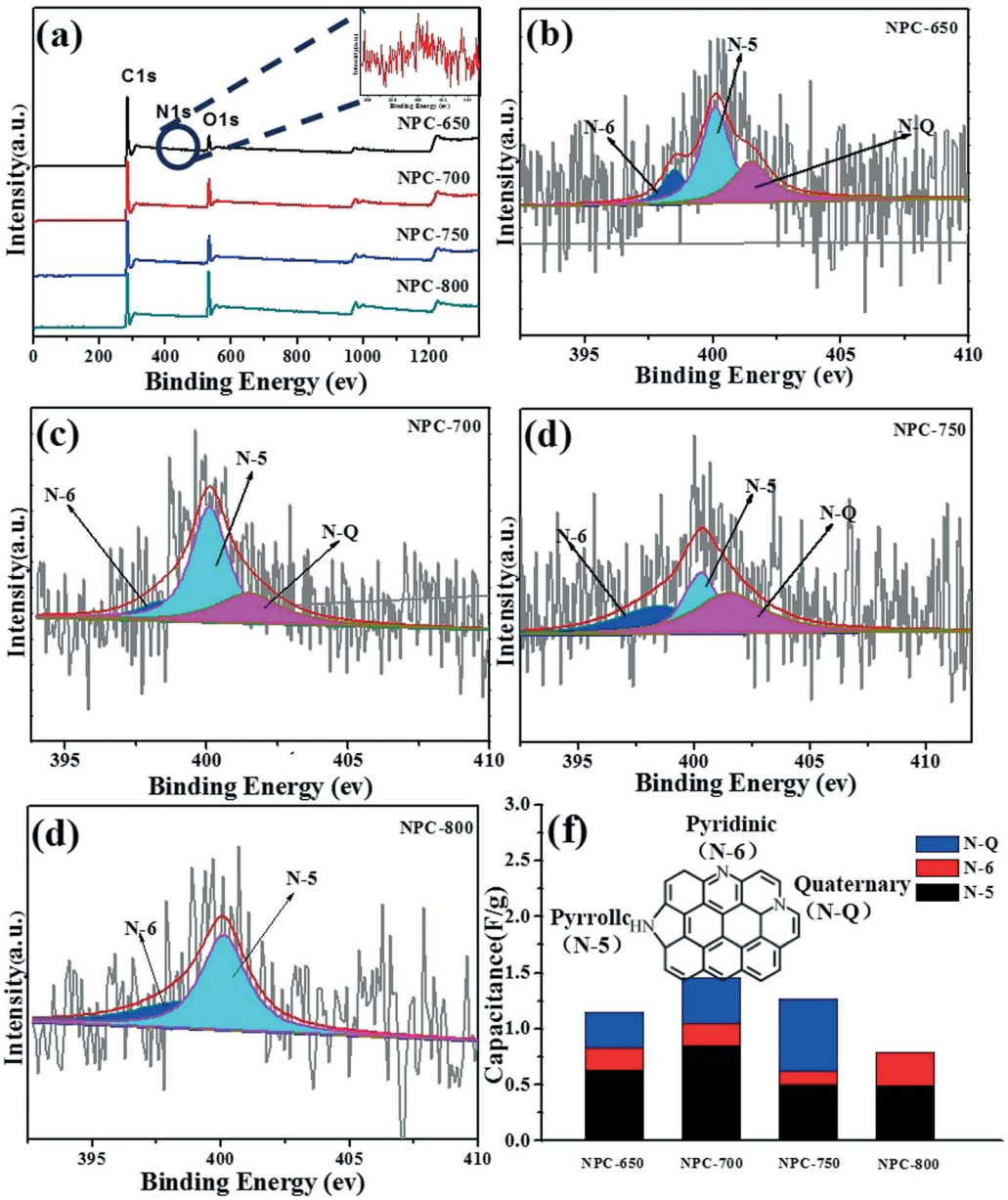

Fig. 3 (a) The full XPS spectra of the four samples, (b ~ f) The contents of three types of nitrogen of four samples.

Table 1 BET area, N-content, and capacitance of four poplar sawdust-derived N-doped porous carbons.

Materials	S_{BET}[a]($m^2 \cdot g^{-1}$)	V[b]($cm^3 \cdot g^{-1}$)	N-content(%)	Cm[c]($F \cdot g^{-1}$)
NPC-650	1005	0.44	1.15	272.9
NPC-700	1245	0.64	1.46	301.5
NPC-750	2149	0.97	1.27	362.0
NPC-800	1855	0.95	0.79	231.0

[a] The specific surface area (S_{BET}) was calculated by the Brunauer–Emmett–Teller (BET) method.
[b] Total pore volume.
[c] Current density at 0.5 $A \cdot g^{-1}$.

be seen that the curves include two stages: -0.8 to -0.4 and -0.4 to 0.2 V. The electric double-layer capacitance plays a leading role in the former, while the electric double-layer capacitance and faradaic capacitance work together in the latter.[65] Figure 6b shows the specific capacitance at different current densities in three-electrode. It can be noted that the composites exhibit a much higher value than NPC, especially at a high current density, which may be related to the increase of mesopore that is beneficial for the diffusion of electrolyte ions.

Figure 6c shows the CV curves of the NPC/PANI at sweeping rates from 5 to 100 $mV \cdot s^{-1}$. Even at a high scan rate of 100 $mV \cdot s^{-1}$, and the CV curve still remains rectangular-like shape, suggesting good rate performance.[57] The inset in Figure 6c displays the CV curves of NPC/PANI in different voltage windows at 25 $mV \cdot s^{-1}$,

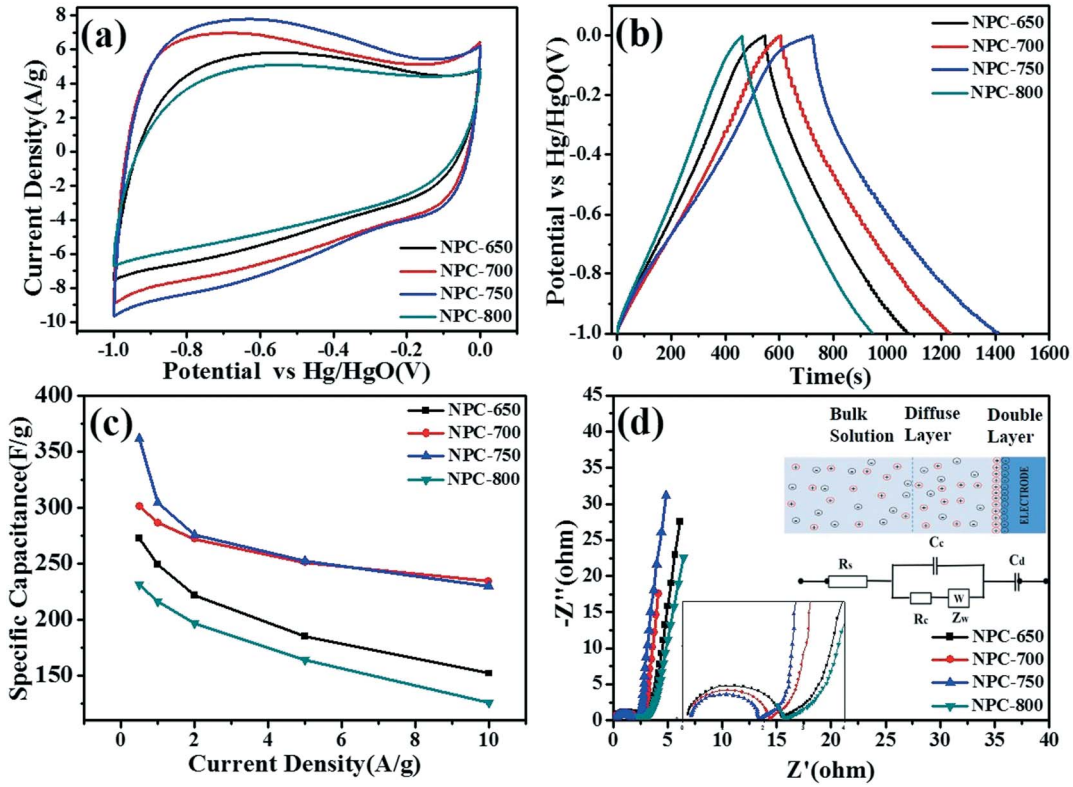

Fig. 4 Electrochemical properties of four poplar sawdust-derived nitrogen-doped porous carbons. (a) Cyclic voltammograms at a scan rate of 25 mV·s $^{-1}$, (b) Galvanostatic charge–discharge at a current density of 0.5 A·g $^{-1}$, (c) Specific capacitance at different current densities, (d) Nyquist impedance plots and equivalent circuit model.

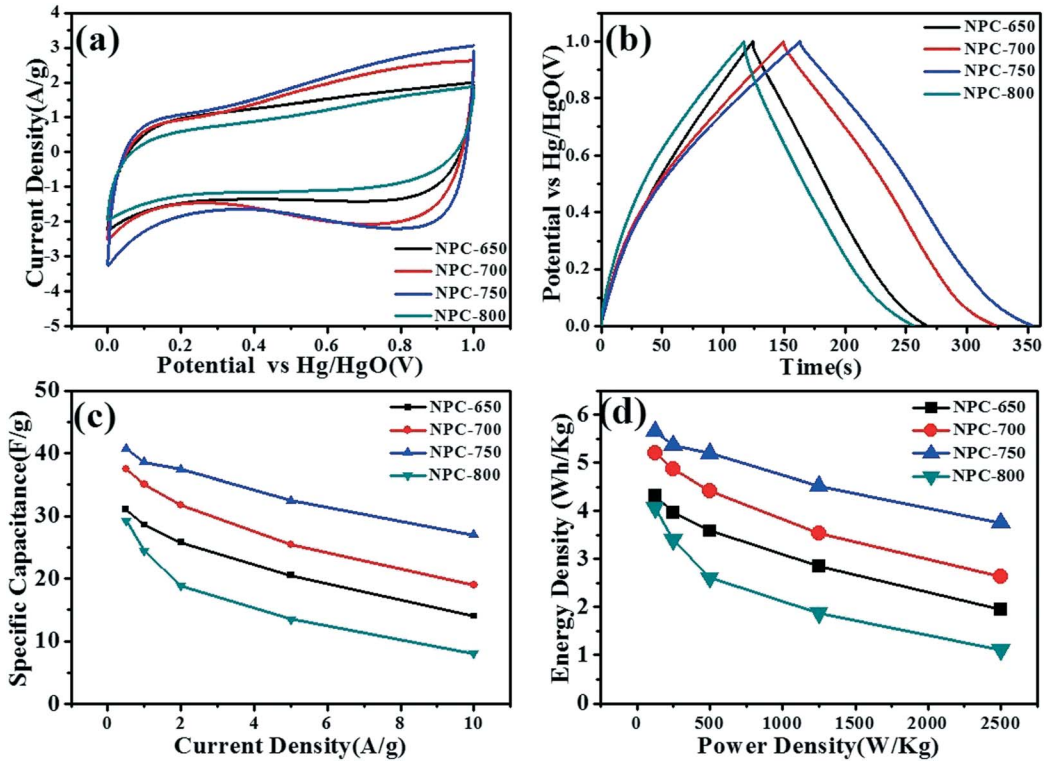

Fig. 5 Electrochemical properties of four poplar sawdust-derived N-doped porous carbons in a two-electrode setup. (a) Cyclic voltammograms at a scan rate of 25 mV·s^{-1} , (b) Galvanostatic charge–discharge at a current density of 0.5 A·g^{-1}. (c) Specific capacitance at different current densities, and (d) Ragone plot.

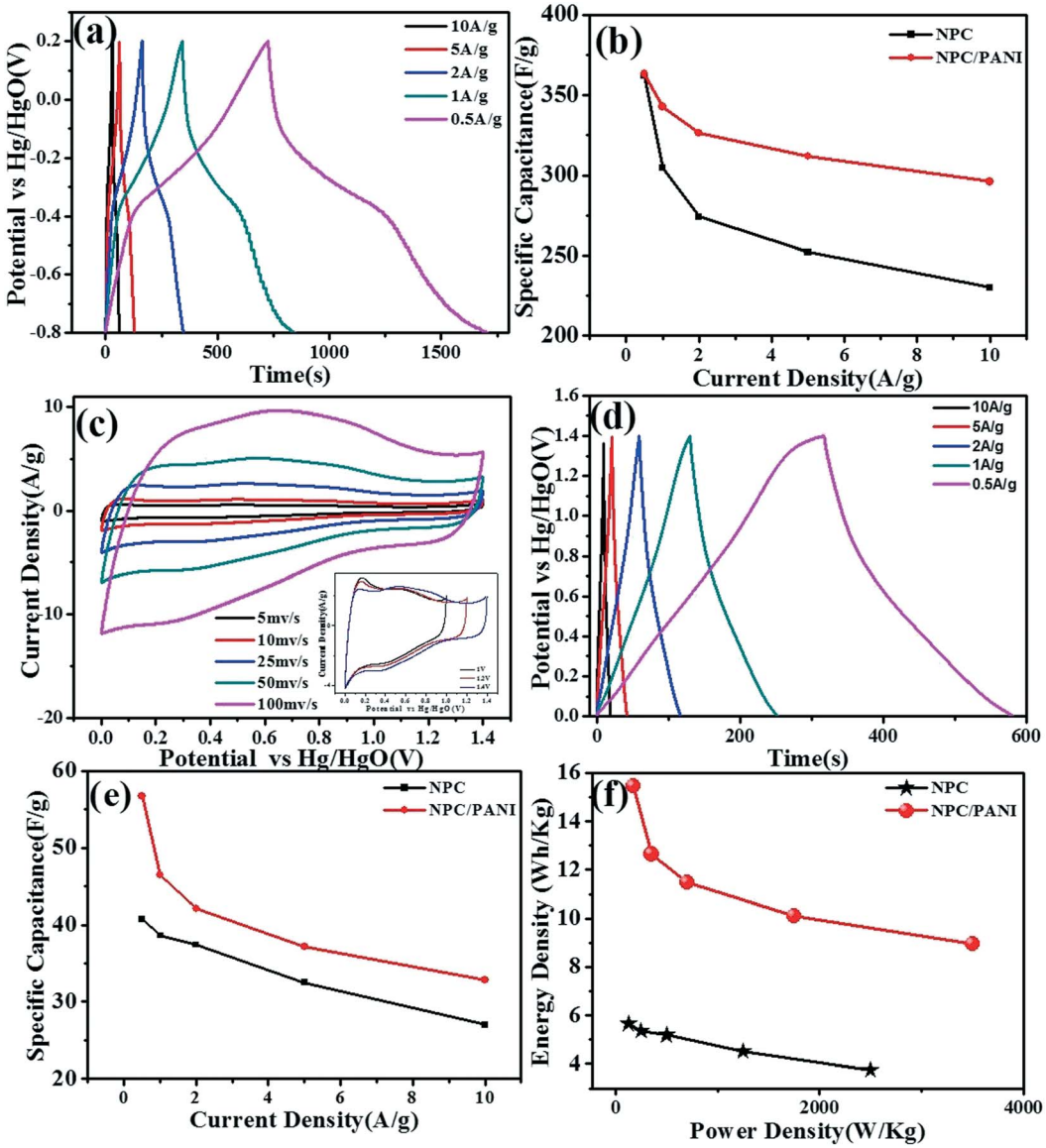

Fig. 6 Electrochemical properties of NPC and NPC/PANI. (a) Galvanostatic charge–discharge of NPC/PANI at different current densities and (b) Specific capacitance at different current densities in a three-electrode setup. (c) Cyclic voltammograms curves at different potential window at 25 $mV{\cdot}s^{-1}$(inset). The Cyclic voltammograms curves at different scan rates and (d) Galvanostatic charge–discharge curves at different current densities of NPC/PANI in a two-electrode setup. (e) Specific capacitance at different current densities, and (f) Ragone plot of NPC and NPC/PANI in a two-electrode setup.

where the composite exhibits a stable voltage window at 0–1.4 V. When the potential is much higher, oxygen evolution occurs.[66] Figure 6d and 6e show the galvanostatic charge–discharging curves and specific capacitance at different current densities, respectively. Based on Figure 6d and 6e, the energy density and power density of composites can be obtained and shown in Figure 6f. The maximum energy density of the NPC/PANI composite is 15.45 $Wh{\cdot}kg^{-1}$ and maximum power density is 3500 $W{\cdot}kg^{-1}$, much higher than 5.66 $Wh{\cdot}kg^{-1}$ and 2500 $W{\cdot}kg^{-1}$ of NPC, respectively. As expected, combination of NPC and PANI greatly improves the capacitance performance of NPC, which is attributed to the synergistic effect of the electric double-layer capacitance and Faradaic capacitance from the NPC and PANI combination, and the interconnected mesopores, which can provide a highly conductive pathway and much easier accessibility for the electrolyte ions during the rapid charge/discharge processes. These results suggest that the combination of NPC and PANI is a promising strategy for developing the high performance supercapacitor.

3. Conclusions

In summary, we used the biomass poplar sawdust as a precursor and KOH as activation agent to successfully prepare the nitrogen-doped porous carbons (NPC) and the NPC/polyaniline (PANI) composites. By optimizing the carbonization temperature, we find the NPC-750 sample shows a highest specific capacitance of 362 $F{\cdot}g^{-1}$ in 6 M KOH among the four samples, due to its large specific surface area of 2149 $m^2{\cdot}g^{-1,}$ and suitable pore size distribution and

high graphitization degree. Further investigations indicate that NPC/PANI composite exhibits a much higher specific capacitance of 312 $F{\cdot}g^{-1}$, a wider voltage range of 0-1.4 V and a much higher energy density of 15.45 $Wh{\cdot}kg^{-1}$, compared to 252 $F{\cdot}g^{-1}$ at 5 $A{\cdot}g^{-1}$, the voltage of 0-1 V and 5.66 $Wh{\cdot}kg^{-1}$ of NPC sample. In short, this work provides a green and environmentally friendly method to convert waste biomass into nitrogen-doped porous carbons and NPC/PANI composite for energy storage applications, and reveals that the integrating NPC and PANI into a composite is a promising strategy for developing the high performance supercapacitor electrode materials.

Acknowledgements

This work is supported by National Science Fund for Distinguished Young Scholars (No. 21625601) and Outstanding Talent Fund from BUCT.

References

1 L. Yang, X. Zeng, W. Wang and D. Cao, *Adv. Funct. Mater.*, 2018, **28**, 1704537.
2 L. Yang, X. Zeng, D. Wang and D. Cao, *Energy Storage Mater.*, 2018, **12**, 277–283.
3 M. W. And and R. J. Brodd, *Chem. Rev.*, 2005, **105**, 4245–4270.
4 A. G. Pandolfo and A. F. Hollenkamp, *J.Power Sources*, 2006, **157**, 11–27.
5 D. W. Wang, F. Li, M. Liu, G. Q. Lu and H. M. Cheng, *Angew. Chem. Int. Ed. Engl.*, 2008, **47**, 373–376.
6 X. Yang, D. Wu, X. Chen and R. Fu, *J. Phys. Chem. C*, 2010, **114**, 8581–8586.
7 D. Bhattacharjya and J. S. Yu, *J. Power Sources*, 2014, **262**, 224–231.
8 Z. Xiang, D. Wang, Y. Xue, L. Dai, J. F. Chen and D. Cao, *Sci. Rep.*, 2015, **5**, 8307–8314.
9 G. Wang, L. Zhang and J. Zhang, *ChemInform*, 2012, **41**, 797–828.
10 V. Augustyn, P. Simon and B. Dunn, *Energy Environ. Sci.*, 2014, **7**, 1597–1614.
11 L. F. Chen, X. D. Zhang, H. W. Liang, M. Kong, Q. F. Guan, P. Chen, Z. Y. Wu and S. H. Yu, *ACS Nano*, 2012, **6**, 7092–7102.
12 B. E. Conway, V. Birss and J. Wojtowicz, *J.Power Sources*, 1997, **66**, 1–14.
13 E. Raymundo-Piñero, F. Leroux and F. Béguin, *Adv. Mater.*, 2006, **18**, 1877–1882.
14 H. Ji, X. Zhao, Z. Qiao, J. Jung, Y. Zhu, Y. Lu, L. L. Zhang, A. H. Macdonald and R. S. Ruoff, *Nat. Commun.*, 2014, **5**, 163–180.
15 J. Wang, L. Shen, B. Ding, P. Nie, H. Deng, H. Dou and X. Zhang, *RSC Adv*, 2014, **4**, 7538–7544.
16 J. Kalupson, D. Ma, C. A. Randall, R. Rajagopalan and K. Adu, *J. Phys. Chem. C*, 2014, **118**, 2943–2952.
17 N. Liu, J. Shen and D. Liu, *Microporous Mesoporous Mater.*, 2013, **167**, 176–181.
18 X. Zang, P. Li, Q. Chen, K. Wang, J. Wei, D. Wu and H. Zhu, *J. Appl. Phys.*, 2014, **115**, 024304–024305.
19 Y. Wang, Z. Shi, Y. Huang, Y. Ma, C. Wang, M. Chen and Y. Chen, *J. Phys. Chem. C*, 2009, **113**, 13103–13107.
20 P. C. Gao, W. Y. Tsai, B. Daffos, P. L. Taberna, C. R. Pérez, Y. Gogotsi, P. Simon and F. Favier, *Nano Energy*, 2015, **12**, 197–206.
21 S. Zhong, C. Zhan and D. Cao, *Carbon*, 2015, **85**, 51–59.
22 A. Borenstein, O. Hanna, A. Ran, S. Luski, T. Brousse and D. Aurbach, *J. Mater. Chem. A*, 2017, **5**.
23 R. Rahimi, M. Ochoa, A. Tamayol, S. Khalili, A. Khademhosseini and B. Ziaie, *ACS Appl. Mater. Inter.*, 2017, **9**.
24 F. O. Agyemang, G. M. Tomboc, S. Kwofie and H. Kim, *Electrochim. Acta*, 2017.
25 M. Qorbani, T. Chou, Y. H. Lee, S. Samireddi, N. Naseri, A. Ganguly, A. Esfandiar, C. H. Wang, L. C. Chen and K. H. Chen, *J. Mater. Chem. A*, 2017, **5**.
26 H. R. Naderi, P. Norouzi and M. R. Ganjali, *App. Sur. Sci.*, 2016, **366**, 552–560.
27 J. Deng, M. Li and Y. Wang, *Green Chem.*, 2016, **18**, 4824–4854.
28 M. Sevilla and R. Mokaya, *Energy Environ. Sci.*, 2014, **7**, 13831–13837.
29 L. Xie, G. Sun, F. Su, X. Guo, Q. Kong, X. Li, X. Huang, L. Wan, W. Song, K. Li, C. Lv and C.-M. Chen, *J. Mater. Chem. A*, 2016, **4**, 1637–1646.
30 S. Xu, Y. Lv, X. Zeng and D. Cao, *Chem. Eng. J.*, 2017, **323**, 502–511.
31 L. Yang, Y. Lv and D. Cao, *J. Mater. Chem. A*, 2018, **6**, 3926–3932.
32 H. Yu, A. Fisher, D. Cheng and D. Cao, *ACS Appl. Mater. Inter.*, 2016, **8**, 21431–21439.
33 R. Wang, P. Wang, X. Yan, J. Lang, C. Peng and Q. Xue, *ACS Appl. Mater. Inter.*, 2012, **4**, 5800–5806.
34 H. Jiang, C. Li, T. Sun and J. Ma, *Nanoscale*, 2012, **4**, 807–812.
35 J. Li, Y. Ren, Z. Ren, S. Wang, Y. Qiu and J. Yu, *J. Mater. Chem. A*, 2015, **3**, 23307–23315.
36 H.-J. Liu, X.-M. Wang, W.-J. Cui, Y.-Q. Dou, D.-Y. Zhao and Y.-Y. Xia, *J. Mater. Chem.*, 2010, **20**, 4223–4230.
37 M.-C. Liu, L.-B. Kong, P. Zhang, Y.-C. Luo and L. Kang, *Electrochim. Acta*, 2012, **60**, 443–448.
38 M. Zhou, F. Pu, Z. Wang and S. Guan, *Carbon*, 2014, **68**, 185–194.
39 W. Sun, S. M. Lipka, C. Swartz, D. Williams and F. Yang, *Carbon*, 2016, **103**, 181–192.
40 H. Wang, Z. Li, J. K. Tak, C. M. B. Holt, X. Tan, Z. Xu, B. S. Amirkhiz, D. Harfield, A. Anyia, T. Stephenson and D. Mitlin, *Carbon*, 2013, **57**, 317–328.
41 P. Yu, Z. Zhang, L. Zheng, F. Teng, L. Hu and X. Fang, *Adv. Energy Mater.*, 2016, **6**, 1601111.
42 D. Kang, Q. Liu, J. Gu, Y. Su, W. Zhang and D. Zhang, *ACS Nano*, 2015, **9**, 11225.
43 Y. Huang, L. Peng, Y. Liu, G. Zhao, J. Y. Chen and G. Yu, *ACS Appl. Mater. Inter.*, 2016, **8**, 15205–15215.
44 B. Song, L. Li, Z. Lin, Z. K. Wu, K. S. Moon and C. P. Wong, *Nano Energy*, 2015, **16**, 470–478.
45 K. Mohd, M. A. Tumelero and A. A. Pasa, *RSC Adv*, 2015, **5**, 62033–62039.
46 Y. G. Wang, H. Q. Li and Y. Y. Xia, *Adv. Mater.*, 2010, **18**, 2619–2623.

47 V. Gupta and N. Miura, *Electrochim. Acta*, 2007, **52**, 1721–1726.
48 L. Li, H. Song, Q. Zhang, J. Yao and X. Chen, *J. Power Sources*, 2009, **187**, 268–274.
49 S. Uppugalla, U. Male and P. Srinivasan, *Electrochim. Acta*, 2014, **146**, 242–248.
50 Z. Li, Z. Xu, H. Wang, J. Ding, B. Zahiri, C. M. B. Holt, X. Tan and D. Mitlin, *Energy Environ. Sci.*, 2014, **7**, 1708–1718.
51 A. C. Ferrari, *Solid State Commun.*, 2007, **143**, 47–57.
52 M. A. Lillo-Ródenas, D. Cazorla-Amorós and A. Linares-Solano, *Carbon*, 2003, **41**, 267–275.
53 K. S. W. Sing, *Pure Appl. Chem.*, 2009, **57**, 603–619.
54 Z. Y. Jin, A. H. Lu, Y. Y. Xu, J. T. Zhang and W. C. Li, *Adv. Mater.*, 2014, **26**, 3700–3705.
55 Z. Xiang, D. Cao, L. Huang, J. Shui, M. Wang and L. Dai, *Adv. Mater.*, 2014, **26**, 3315–3320.
56 M. Seredych, D. Hulicova-Jurcakova, Q. L. Gao and T. J. Bandosz, *Carbon*, 2008, **46**, 1475–1488.
57 Y. Li, G. Wang, T. Wei, Z. Fan and P. Yan, *Nano Energy*, 2016, **19**, 165–175.
58 Y. Deng, Y. Xie, K. Zou and X. Ji, *J. Mater. Chem. A*, 2016, **4**, 1144–1173.
59 sS. Shrestha, S. Asheghi, J. Timbro and W. E. Mustain, *Appl. Catal., A*, 2013, **S464–465**, 233–242.
60 L. Sun, C. Tian, Y. Fu, Y. Yang, J. Yin, L. Wang and H. Fu, *Chem.-Eur. J.*, 2014, **20**, 564–574.
61 N. P. Wickramaratne, J. Xu, M. Wang, L. Zhu, L. Dai and M. Jaroniec, *Chem. Mater.*, 2014, **26**, 2820–2828.
62 S. J. Yang, T. Kim, K. Lee, Y. S. Kim, J. Yoon and R. P. Chong, *Carbon*, 2014, **71**, 294–302.
63 X. Luo and J. J. Davis, *ChemInform*, 2013, **42**, 5944–5962.
64 K. P. Wang and H. Teng, *J. Electrochem. Soc.*, 2007, **154**, A993–A998.
65 J. Yan, T. Wei, B. Shao, Z. Fan, W. Qian, M. Zhang and F. Wei, *Carbon*, 2010, **48**, 487–493.
66 X. Zhao, C. Chen, Z. Huang, L. Jin, J. Zhang, Y. Li, L. Zhang and Q. Zhang, *RSC Adv*, 2015, **5**, 66311–66317.